© 2020. Published by The Company of Biologists Ltd | Journal of Cell Science (2020) 133, jcs243162. doi:10.1242/jcs.243162

RESEARCH ARTICLE

miR-206 enforces a slow muscle phenotype

Kristen K. Bjorkman, Martin G. Guess*, Brooke C. Harrison‡, Michael M. Polmear§, Angela K. Peter¶ and Leslie A. Leinwand**

ABSTRACT

Striated muscle is a highly specialized collection of tissues with contractile properties that vary according to functional needs. Although muscle fiber types are established postnatally, lifelong plasticity facilitates stimulus-dependent adaptation. Functional adaptation requires molecular adaptation, which is partially provided by miRNA-mediated post-transcriptional regulation. miR-206 is a muscle-specific miRNA enriched in slow muscles. We investigated whether miR-206 drives the slow muscle phenotype or is merely an outcome. We found that miR-206 expression increases in both physiological (including female sex and endurance exercise) and pathological conditions (muscular dystrophy and adrenergic agonism) that promote a slow phenotype. Consistent with that observation, the slow soleus muscle of male miR-206-knockout mice displays a faster phenotype than wild-type mice. Moreover, left ventricles of male miR-206 knockout mice have a faster myosin profile, accompanied by dilation and systolic dysfunction. Thus, miR-206 appears to be necessary to enforce a slow skeletal and cardiac muscle phenotype and to play a key role in muscle sexual dimorphisms.

KEY WORDS: miR-206, miRNA, Skeletal muscle, Heart, Sexual dimorphism

INTRODUCTION

Skeletal muscle is a highly organized contractile tissue that comprises 40% of human body mass (Janssen et al., 2000). Muscle subgroups are further specialized to perform a diverse array of functions, such as chewing, focusing and moving the eye, breathing, maintaining body posture, and both burst and sustained movements. To meet these various demands, different muscle types are characterized by different metabolic and contractile machinery. Oxidative myofibers are more fatigue resistant and have higher mitochondrial content, to facilitate β-oxidation. They can be further subdivided into slow oxidative and fast oxidative myofibers. Slow oxidative fibers are also called type I fibers due to expression of type I (β)-myosin heavy chain (MyHC; MYH7), a member of the sarcomeric MyHC protein family, which ultimately confers contractile properties to the muscle. Fast oxidative fibers express type IIa (MYH2), IIx (MYH1), or a mixture of those two faster MyHCs. They also are more oxidative than type I fibers, presumably to accommodate the greater ATP demands of types IIa and IIx MyHCs compared to type I (Chemello et al., 2019). Fast glycolytic myofibers fatigue more easily and rely on glycolysis for energy production. Smaller mammals express the fastest MyHC (type IIb; MYH4) or a IIx/IIb mixture to promote higher contraction speed, while larger mammals do not express the type IIb myosin protein (Pereira Sant'Ana et al., 1997).

Although fiber types are established shortly after birth (Gokhin et al., 2008), adult skeletal muscle retains remarkable plasticity in order to adapt to changing demands. In addition to tuning performance, muscle is a metabolically demanding tissue that is critical to maintaining body-wide homeostasis due to the balance of energy substrate utilization. Physiological stimuli, such as short sprint versus endurance exercise training, shifts muscles to a more glycolytic or more oxidative phenotype, respectively (Allen et al., 2001; Andersen and Henriksson, 1977; Ross and Leveritt, 2001). Muscle unloading due to a variety of stimuli typically results in a more glycolytic profile (Caiozzo et al., 1998; Harrison et al., 2003; McCarthy et al., 1997). Certain pathological states, including muscular dystrophy, result in a shift to more oxidative/slow fibers, in part because fast fibers are more susceptible to damage (Webster et al., 1988). Finally, although understudied, evidence from rodents to humans suggests that many female muscles are slower than their male counterparts (Haizlip et al., 2015; Janssen et al., 2000).

Cardiomyocytes, the contractile cells in cardiac muscle, express two MyHCs in mammals: the same β-MyHC found in type I skeletal muscle fibers as well as the faster, cardiac-restricted α-MyHC (MYH6). There is also evidence that female cardiac muscle is slower than male muscle (Patrizio et al., 2013; Trexler et al., 2017). While most mammalian species express both MyHCs in the heart, the α:β ratio varies between species but is tightly controlled within a species. Mice typically express >99% α-MyHC while humans express >90% β-MyHC (Izumo et al., 1987; Krenz and Robbins, 2004; Miyata et al., 2000; Sadayappan et al., 2009). However, β-MyHC levels increase in most types of heart disease, regardless of species (Miyata et al., 2000; Nadal-Ginard and Mahdavi, 1989; Nakao et al., 1997). This is presumably a compensatory response as the slower, more energetically efficient β-MyHC may be more suited to the metabolic stress that typifies many forms of heart disease (Hoyer et al., 2007). However, the accompanying reduction in contractility ultimately renders this a maladaptive long-term response.

Tuning the gene expression profiles in these muscle types occurs through a coordinated transcriptional and post-transcriptional network. miRNA-mediated post-transcriptional regulation is a key event in muscle development: skeletal muscle-specific knockout of Dicer, which prevents all miRNA maturation in this tissue, is embryonic lethal (O'Rourke et al., 2007). Several miRNAs have been shown to modulate muscle fiber type. For example, double knockout of the two miR-133a genes doubles the percentage of type I fibers at the expense of type II fibers in the soleus, suggesting it

Department of Molecular, Cellular, and Developmental Biology, BioFrontiers Institute, University of Colorado Boulder, 3415 Colorado Ave., UCB596, Boulder, CO 80303, USA.
*Present address: Roche Diagnostics, Basel, Switzerland. ‡Present address: Forma Therapeutics, Watertown, Massachusetts, United States. §Present address: United States Army, William Beaumont Army Medical Center/Texas Tech University Health Sciences Center, El Paso, Texas, United States. ¶Present address: Edgewise Therapeutics, Boulder, Colorado, United States.

**Author for correspondence (Leslie.Leinwand@colorado.edu)

K.K.B., 0000-0002-9540-6657; L.A.L., 0000-0003-1470-4810

Handling Editor: Maria Carmo-Fonseca
Received 31 December 2019; Accepted 25 June 2020

Journal of Cell Science (2020) 133, jcs243162. doi:10.1242/jcs.243162

enforces a fast program (Liu et al., 2011). In addition, miR-27a promotes a fast oxidative (type IIa) phenotype, while miR-499 and miR-208b promote the type I slow phenotype (Chemello et al., 2019; van Rooij et al., 2009). Along with the miR-208 and -499, and the miR-133 family, the miR-1/206 family is also predominantly expressed in muscle (Ma et al., 2015; McCarthy, 2008; Mitchelson, 2015). Interestingly, although miR-206 expression is low in non-muscle tissues, its levels decrease in numerous cancers. Moreover, ectopic miR-206 expression can inhibit tumor cell growth and induce apoptosis, suggesting functional relevance (Nohata et al., 2012). In the basal state, miR-206 is most highly enriched in slow muscle fibers (Boettger et al., 2014; Williams et al., 2009). miR-206 is also upregulated in fast muscle in several pathological settings, including the chronic, progressive damage associated with amyotrophic lateral sclerosis (ALS) and Duchenne muscular dystrophy (DMD), as well as acute chemical injury from cardiotoxin injection (Liu et al., 2012; Williams et al., 2009; Yuasa et al., 2008). In conditions such as spaceflight and aging, which are associated with mixed fiber type muscle shifting towards a faster profile, miR-206 levels decrease (Allen et al., 2009; Hamrick et al., 2010; Kim et al., 2014). Although miR-206 is induced after myocardial infarction (Dong et al., 2009; Limana et al., 2011; Shan et al., 2009), it is unclear whether it is important in the heart at baseline. Notably, despite a general sex difference in muscle fiber types, it is not known whether biological sex influences miR-206 expression. Thus, we sought to determine in both sexes whether the miR-206 slow muscle enrichment is an outcome or a driver of the oxidative phenotype.

RESULTS

miR-206 is associated with a slow-twitch muscle phenotype and is higher in female fast muscles

We measured miR-206 levels in three mouse lower hindlimb muscles with different fiber type compositions. In both males and females, we found a stepwise increase in miR-206 expression from the fastest muscle [tibialis anterior (TA)] to a mixed fiber type muscle [gastrocnemius and plantaris (GP)] to the slowest muscle [soleus (SOL)]. As shown in Fig. 1A, there was an ∼30-fold

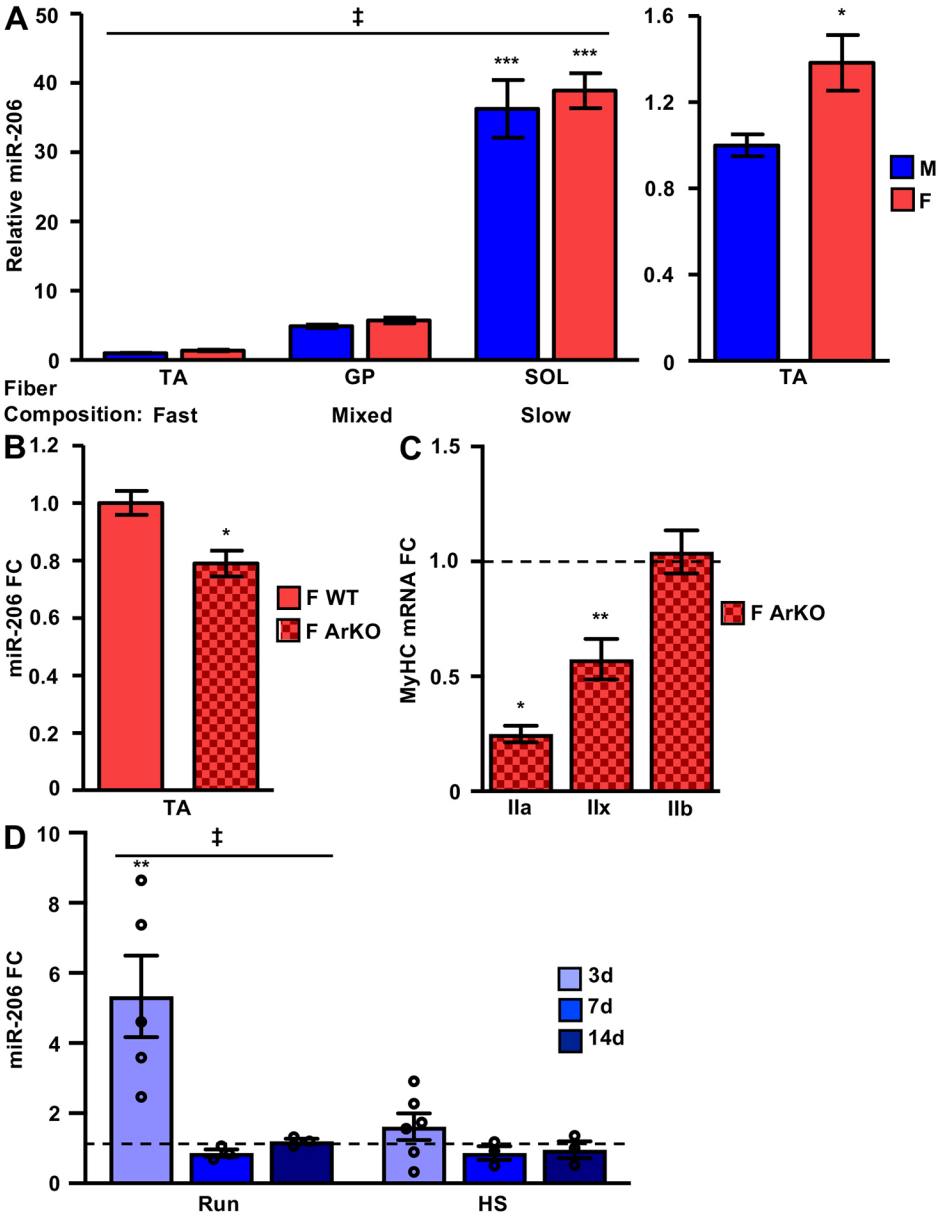

Fig. 1. miR-206 expression is highest in slow twitch muscle and is upregulated with endurance exercise. (A) miR-206 levels are highest in slow muscles in both sexes (left panel) but higher in female (F) compared to male (M) TA (right panel). We assessed miR-206 expression by qPCR in tibialis anterior (TA), gastrocnemius and plantaris (GP), and soleus (SOL) from male and female mice. Expression relative to male TA is presented. *n* values are: 8, M TA; 8, F TA; 9, M GP; 8, F GP; 10, M SOL; 8, F SOL. Two-way ANOVA indicated a significant effect from muscle group (line with ‡; $P \leq 0.001$). Asterisks indicate Bonferroni post-test results. ***$P \leq 0.001$ SOL vs TA or vs GP within each sex, *$P \leq 0.015$ F vs M TA. (B) miR-206 expression is lower in TAs from aromatase-null (ArKO) compared to WT female mice. Fold change (FC) relative to WT F TA from qPCR is presented. $n=6$ in both groups. Student's *t*-test indicated a significant difference between genotypes. *$P=0.014$. (C) Slower type II myosins are expressed at lower levels in TAs from F ArKO compared to WT mice. mRNA levels were assessed by qPCR and normalized to *Acta1*. FC is relative to that in WT F TA (line at $y=1$). Student's *t*-test indicated a significant difference between genotypes. *$P \leq 0.05$, **$P \leq 0.01$ ArKO vs WT. *n* values are: 6, WT; 7, ArKO. (D) In male mice, miR-206 expression increased by 3 days after initiating voluntary cage wheel running and then returned to baseline, but it did not change upon muscle unloading through hindlimb suspension (HS). FC relative to that in normal cage activity controls (line at $y=1$) is presented. *n* values are: 6, control; 5, 3 days run; 3, 7 days run; 3, 14 days run; 6, 3 days HS; 3, 7 days HS; 3, 14 days HS. One-way ANOVA indicated a significant effect from running (line with ‡; $P \leq 0.01$). Asterisks indicate Tukey's post-test results. **$P \leq 0.01$, 3 days run vs control. Error bars show s.e.m.

Journal of Cell Science (2020) 133, jcs243162. doi:10.1242/jcs.243162

enrichment in SOL compared to TA. Interestingly, there were significantly higher miR-206 levels in female TA compared to male TA (Fig. 1A, right panel), which supports our previous observation that the female TA contains a greater fraction of slow fibers than the male TA (Haizlip et al., 2015). miR-206 expression was not sexually dimorphic in either the GP or SOL. There was also no sex difference in the expression of the other myomiRs (miR-1, miR-133b or miR-133a) in the TA (Fig. S1A). Since miR-206 levels can differentially respond to ligands binding to different estrogen receptors in breast cancer cells (Adams et al., 2007), we assessed a potential hormonal basis for the sex difference in the TA by examining miR-206 levels in female aromatase (also known as CYP19A1) knockout (ArKO) mice, which do not produce any estrogen. In ArKO TA, we observed a significant 1.3-fold reduction in miR-206 levels (Fig. 1B), while miR-1, -133b, and -133a were unaffected (Fig. S1B), suggesting a miR-206-specific phenomenon. miR-206 levels were not altered in either the ArKO GP or SOL (Fig. S1C). In light of the lower miR-206 levels in the female ArKO TA, we considered whether there might be a corresponding shift in myosin heavy chain (MyHC) expression to suggest a shift towards a faster twitch phenotype. The adult MyHCs can be ranked from slowest to fastest with respect to ATPase activity: β (type I slow), IIa, IIx and IIb (Resnicow et al., 2010). While β-MyHC mRNA is not abundant enough in the TA to be reliably interpreted, we found 4-fold and 1.7-fold reductions in MyHC IIa and IIx expression, respectively, with no change in MyHC IIb mRNA levels (Fig. 1C). Thus, the slower the type II myosin, the greater the decrease in the female ArKO TA.

As it is well known that endurance exercise induces a shift towards a slow twitch phenotype (Allen et al., 2001; Andersen and Henriksson, 1977), we examined miR-206 expression in the TAs of male WT mice during adaptation to voluntary wheel running. miR-206 levels increased 5.3-fold after 3 days of exercise but were not different from sedentary levels after 7 or 14 days of running (Fig. 1D). Hindlimb suspension, a model of muscle disuse that can induce a fast-twitch shift, did not result in changes in miR-206 expression (Fig. 1D).

We next evaluated whether miR-206 expression responds to pathological muscle stimuli that shift typical fast muscles to a slower phenotype. One characteristic of Duchenne muscular dystrophy (DMD) is selective sparing of slow muscle and disproportionate loss of fast muscle (Webster et al., 1988). In addition, the damage-induced regeneration in the earlier phases of the disease is accompanied by re-expression of embryonic MyHC, one of the slowest sarcomeric myosins (Ciciliot and Schiaffino, 2010; Resnicow et al., 2010). In agreement with both of these observations, in the *mdx4cv* mouse model of DMD, we saw induction of miR-206 in both TA and GP with no change in the SOL (Fig. 2A), which is in agreement with previous reports (Guess et al., 2015; Liu et al., 2012). Consistent with this, miR-206 was induced in human DMD vastus lateralis biopsies, a normally mixed fiber type thigh muscle (Fig. 2B). Muscle regeneration in response to acute injury also includes a transient period of slow embryonic MyHC (MYH3) re-expression before re-establishing the normal adult muscle phenotype. Fig. S1D,E illustrate this early, marked increase in embryonic MyHC mRNA as well as the initial depletion of the adult fast MyHC, IIx, followed by recovery of both of their levels by day 14.

We also found a stepwise increase in miR-206 expression during a 2-week regeneration time course in $BaCl_2$-injured TA (Fig. 2C). This increase seems likely due to transcriptional activation, as we observed a robust induction of the primary miR-206 transcript that preceded peak levels of the mature miRNA and then decreased towards basal levels as regeneration proceeded (Fig. 2D). We assessed transcriptional induction directly and *in vivo* by injecting a luciferase reporter gene controlled by a 200-bp upstream miR-206 enhancer and a minimal promoter (Fig. S2A) into GP that we subsequently injured with $BaCl_2$. During the regeneration time course, we saw a peak in luciferase activity at 3 days post-injury, consistent with the peak in endogenous pri-miR-206 levels (Fig. 2E). This behavior was dependent on the miR-206 enhancer, as there was no injury response from a construct with just a basal promoter driving luciferase (Fig. 2E; Fig. S2D). We also saw that this enhancer region responded to endogenous myogenic cues in differentiating C2C12 mouse myoblasts and in 10T1/2 mouse fibroblasts transfected with each of the four muscle regulatory factors (MyoD, myogenin, MRF4 and Myf5; Fig. S2B,C). MyoD is known to bind this region (Rao et al., 2006; Sweetman et al., 2008), and there are five E-boxes with the generic consensus CANNTG (Fig. S2A). A more refined muscle consensus site has been proposed that has a more specific core hexamer [CA(C/G)(C/G)TG] and extended flanking sequence (Yutzey and Konieczny, 1992). We found that the first, second and fifth E-boxes conform well to this muscle consensus but the third and fourth do not (Fig. S2E). In agreement, only the muscle consensus E-boxes are conserved in the human genome, and mutation of only these E-boxes abolished the reporter response to C2C12 differentiation (Fig. S2F). Moreover, a reporter construct with the orthologous human region is also induced with mouse C2C12 differentiation cues, buttressing the assertion that only the three conserved E-boxes are bona fide sites of transcriptional activation (data not shown). This region has also been reported to function as a transcriptional enhancer dependent on the same E-boxes in neonatal rat cardiomyocytes (Yang et al., 2015).

miR-206 deletion results in a slow-to-fast muscle switch

We next investigated whether miR-206 expression is an outcome or a driver of the slow muscle phenotype by examining the miR-206 knockout mouse (206KO) (Williams et al., 2009). In this mouse, the miR-206 precursor stem loop is specifically deleted without impacting the downstream miRNA, miR-133b, or exons of the long noncoding RNA, linc-MD1. In the original work from the Olson group, young 206KO mice were found to be grossly normal, so we examined 6–7-month-old mice to assess whether age would reveal any phenotypes. We found a male-specific increase in SOL mass while the faster TA and GP muscles were unaffected (Fig. 3A; Fig. S3A,B). This effect appears to be specific to lack of miR-206, as we did not observe any compensatory change in the expression of the closely related miR-1 nor any perturbation in the expression of the genetically linked miR-133b (Fig. S3D) or in linc-MD1, the noncoding RNA also generated from this locus (Fig. S3E).

We further characterized the phenotype of the 206KO SOL through cross-sectional area (CSA) analysis and MyHC-based fiber typing. We stained cross-sections with antibodies specific to slow type I (β-MyHC), intermediate type IIa and fast type IIx, as well as laminin, to reveal fiber borders (representative images are shown in Fig. 3B). We measured fiber type-specific CSA and calculated the percentage of fibers that were distributed in 200 μm^2 bins for both WT and 206KO males. Heatmaps display these data in Fig. 3C. We observed that 206KO type I fibers are smaller while 206KO type IIA fibers have a broader size distribution when compared to WT. While IIX fibers are a rarer fiber type in the SOL, there was a noticeable shift towards larger fibers in 206KO mice. In all fiber types, the

Journal of Cell Science (2020) 133, jcs243162. doi:10.1242/jcs.243162

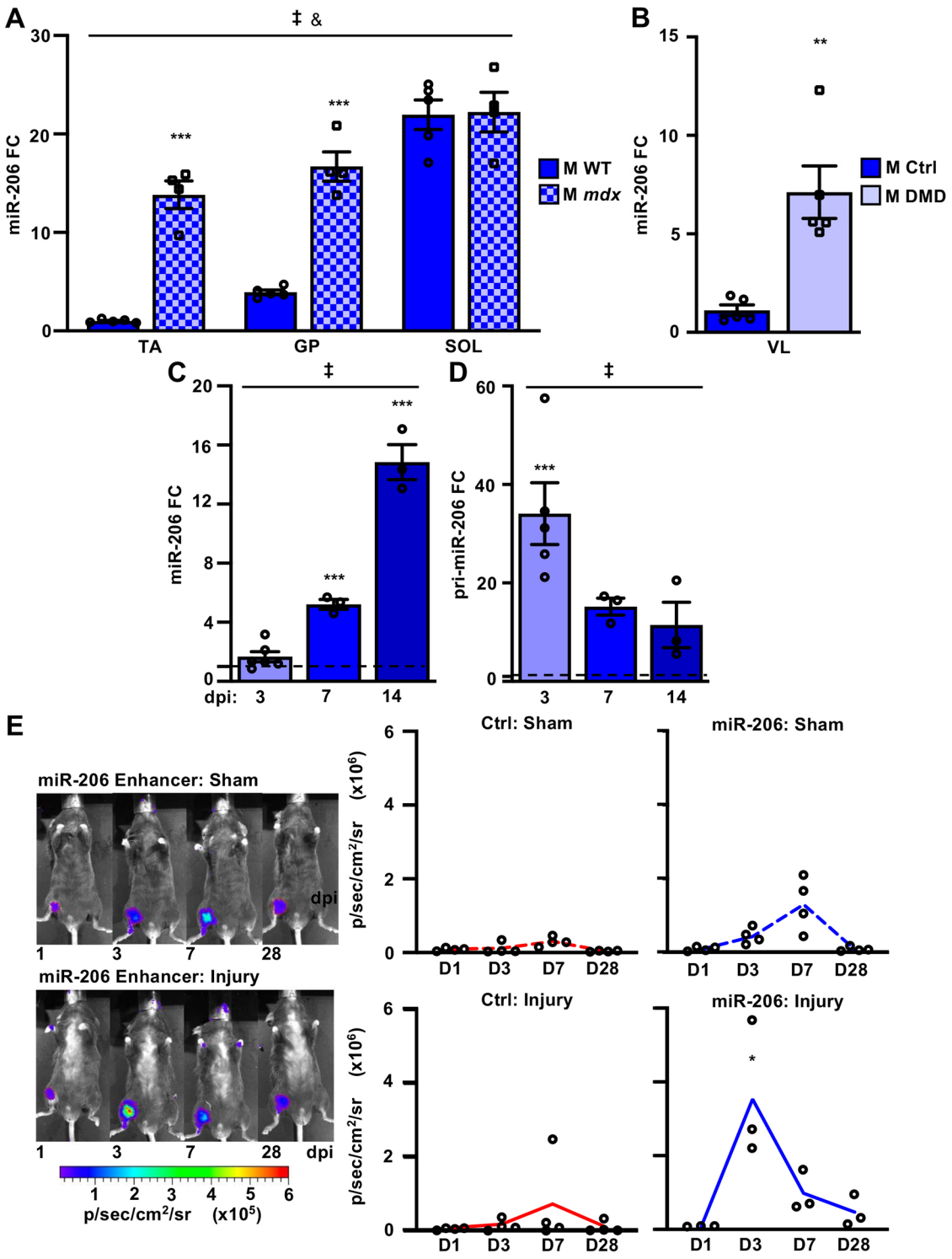

Fig. 2. See next page for legend.

largest size bins are only populated in the 206KO genotype. In analyzing proportions of fiber types, we calculated a 25% decrease in the proportion of type I fibers and a 14% increase in the proportion of type IIA fibers in 206KO mice. We also observed a striking increase in the fraction of fast IIX fibers in 206KO mice. While this was not statistically significant due to inter-animal variability, it is noteworthy (Fig. 3D). Corroborating these fiber typing data, we saw a significant 2.5-fold increase in MyHC IIa and a 3.4-fold increase in MyHC IIx mRNA (Fig. 3E). MyHC IIb was essentially undetectable in the SOL of either genotype (data not shown). Consistent with unchanged female muscle masses, we found no change in MyHC expression in female 206KO SOL (Fig. S3C). While we cannot rule out the possibility of increased total fiber number to account for the greater SOL mass in 206KO males, increased proportion and size of types IIA and IIX fibers could be contributing factors.

Fig. 2. miR-206 is transcriptionally upregulated in pathological conditions that shift fast muscles to a slower phenotype. (A) miR-206 levels are higher in *mdx4cv* TA and GP compared to WT, but are not different in slow SOL of male (M) mice. We measured miR-206 levels as in Fig. 1. *n* values are: 5, WT; 4, *mdx4cv*. Two-way ANOVA indicated a significant effect from genotype and muscle group (line with ‡ and &; $P \leq 0.001$). Asterisks indicate Bonferroni post-test results within muscle groups. ***$P \leq 0.001$ *mdx4cv* vs WT. (B) miR-206 levels are higher in vastus lateralis (VL) from male (M) human DMD patients compared to healthy controls. $n=5$ for both groups. Student's *t*-test indicated a significant difference between genotypes. **$P=0.0090$. (C,D) Mature miR-206 (C) and pri-miR-206 (D) levels as measured by qPCR increase in regenerating TA after $BaCl_2$ injury at the indicated days post-injury (dpi). Expression levels relative to the uninjured (PBS-injected) contralateral control TA are presented. Control levels are represented as a dashed line at $y=1$. *n* values are: 5, 3 dpi; 3, 7 dpi; 3, 14 dpi. Two-way ANOVA indicated a significant effect from injury (line with ‡; $P \leq 0.001$). Asterisks indicate Bonferroni post-test results. ***$P \leq 0.001$ vs control. (E) A luciferase reporter gene driven by the miR-206 enhancer is upregulated *in vivo* during muscle regeneration. We injected the miR-206 enhancer reporter construct or the minTATA negative control reporter intravenously into the mouse hindlimb. We subsequently injured the gastrocnemius with $BaCl_2$ ('injury') or injected it with PBS as a control ('sham'). We measured reporter gene activity at days 1, 3, 7 and 28 after injury. Representative images of miR-206 reporter mice are shown. Bioluminescence signal is expressed as photons $(\text{second})^{-1}$ $(\text{cm}^2)^{-1}$ $(\text{steradian})^{-1}$ ($\text{p/s/cm}^2\text{/sr}$). Signal intensity was false colored according to the color bar below. Average signal intensities are plotted to the right. *n* values are 3–4 per group. Student's *t*-test revealed a significant difference at D3 in injured animals injected with the miR-206 reporter (*$P \leq 0.05$) vs control group injected with the same plasmid. Error bars show s.e.m.

To extend our molecular profiling of 206KO soleus, we measured expression levels of RNAs typically enriched in either slow or fast skeletal muscle (Fig. 4). We considered transcription factors, noncoding RNAs, troponin isoforms and metabolic factors in addition to the MyHC signature described above. Amongst transcription factor-encoding genes, we found a 2-fold upregulation of the slow-associated *Mef2c* as well as the fast-associated *Six1* and *Eya1*. We found no change in the expression of the slow-associated miRNAs miR-208b and miR-499 but a 2-fold upregulation of the fast-associated long noncoding RNA linc-MYH. Beyond the MyHC isoform content, contractile properties are also tuned by functionally distinct isoforms of other sarcomere components, including troponins. In skeletal muscle, the *Tnni2* isoform of troponin I is fast-associated while *Tnni1* is slow-associated (Sheng and Jin, 2016). However, we did not see changes in the expression of either isoform. Expression of the slow-associated Ca^{2+}-handling factor *Serca2a* did not change but there was a modest but significant increase in the oxygen-binding protein myoglobin (*Mb*). When we consider these data in conjunction with the MyHC analysis, we see an overall shift towards inducing a fast oxidative muscle phenotype in the absence of miR-206, indicating it is likely to be an enforcer of the slow program.

miR-206 deletion results in cardiac dilation

In a healthy rodent heart, miR-206 levels are typically quite low (Fig. S4A) (Boettger et al., 2014; Kim et al., 2006). However, under pathological conditions, including myocardial infarction (MI), hyperglycemia and genetic dilated cardiomyopathy, miR-206 is induced (Dong et al., 2009; Limana et al., 2011; Shan et al., 2009, 2010; Westendorp et al., 2012). Two MyHC isoforms are expressed in the heart: β-MyHC and the faster α-MyHC. One characteristic of multiple forms of heart disease is a shift towards a greater proportion of β-MyHC. To evaluate whether miR-206 induction extends to other pathological conditions in the heart, we treated wild-type male mice with increasing doses of the β-adrenergic receptor agonist isoproterenol, which chemically models pressure overload. Confirming the pathologic impact of the treatment, we saw increases in heart rate, normalized left ventricular (LV) mass, and the mRNAs encoding the pathologic markers atrial and B-type natriuretic factors (ANF and BNP; also known as NPPA and NPPB, respectively) (Fig. S4B–D). We saw a significant dose-responsive increase in β-MyHC mRNA (Fig. 5A) and in miR-206, the latter of which was induced 4-fold in 45 mg kg^{-1}-treated animals compared to vehicle controls (Fig. 5B).

Therefore, we proceeded to morphologically, functionally and molecularly characterize hearts from 206KO animals. In males, we found a significant 11% increase in normalized LV mass (Fig. 6A) with no change in female LVs (Fig. S5A). Similar to what we found with the SOL, we saw no dysregulation of other myomiRs, including miRs-133b, -1, -208a and -208b (Fig. S6A). Using M-mode echocardiography, we observed significant LV anterior wall thinning with no change in LV posterior wall thickness, as well as chamber dilation during systole in male 206KO mice compared to wild-type controls (Fig. 6B). Consistent with this, M-mode calculations revealed a 59% increase in male 206KO LV systolic volume and an accompanying 17% decrease in ejection fraction and 25% decrease in percent fractional shortening, which were all statistically significant (Fig. 6C). Again, we saw no change in female LV dimensions or function (Fig. S5D,E).

We molecularly assessed the male 206KO LVs by quantitative (q)PCR-based analysis of a suite of mRNAs and miRNAs whose expression is frequently perturbed in a variety of cardiac pathologies (Taegtmeyer et al., 2010; Van Rooij et al., 2006). These include mRNAs encoding ANF and BNP, the skeletal muscle isoform of sarcomeric actin (*Acta1*), the Ca^{2+}-handling factors *Serca2a* and *Pln*, the fetal cardiac transcription factors *Gata4* and *Nkx2.5*, the Nfat target myocyte-enriched calcineurin-interacting protein (*mCip1.4*), the pro-fibrotic collagen 1 (*Col1a1*), and the anti-hypertrophic muscle cytokine myostatin (*Mstn*). Surprisingly, the only changes we observed were a 1.7-fold increase in *Acta1* and a 1.6-fold decrease in *Mstn*, consistent with cardiac pathology and an increase in LV mass, respectively (Fig. S6B). We also observed no significant dysregulation in ten miRNAs previously identified as part of a signature set of miRNAs whose expression levels respond to three different pathologic cardiac stimuli (Fig. S6C) (Van Rooij et al., 2006). However, when we measured MyHC mRNA levels, we saw a significant 1.4-fold induction of the faster cardiac isoform α-MyHC with a 1.3-fold downward trend in the slower β-MyHC (Fig. 6D). Consistent with unchanged LV size and preserved function, we found no change in α- or β-MyHC expression in female 206KO LV (Fig. S5C). This suggests a shift towards a faster cardiac phenotype with pathological functional consequences in the absence of miR-206 expression.

DISCUSSION

We show that miR-206 is essential to enforce a slow muscle program in both skeletal muscle and the heart. In healthy skeletal muscle, miR-206 expression is strongly associated with a slow oxidative phenotype and is significantly higher in the female compared to male TA (Fig. 1A). This aligns with our previous observations that the female TA contains a greater proportion of slow fibers, and that females have a greater, but hormone-dependent, capacity for endurance exercise (Haines et al., 2012; Haizlip et al., 2015). There is likely to be a hormonal component to this expression pattern as aromatase-null females express less miR-206 in the TA than wild-type females (Fig. 1B). Interestingly, estrogen can regulate miR-206 expression levels in breast cancer cells, further reinforcing this hormonal link (Adams et al., 2007). We did not see the same sex bias or response to aromatase deletion in expression of the miR-206 family member miR-1 nor in the

Journal of Cell Science (2020) 133, jcs243162. doi:10.1242/jcs.243162

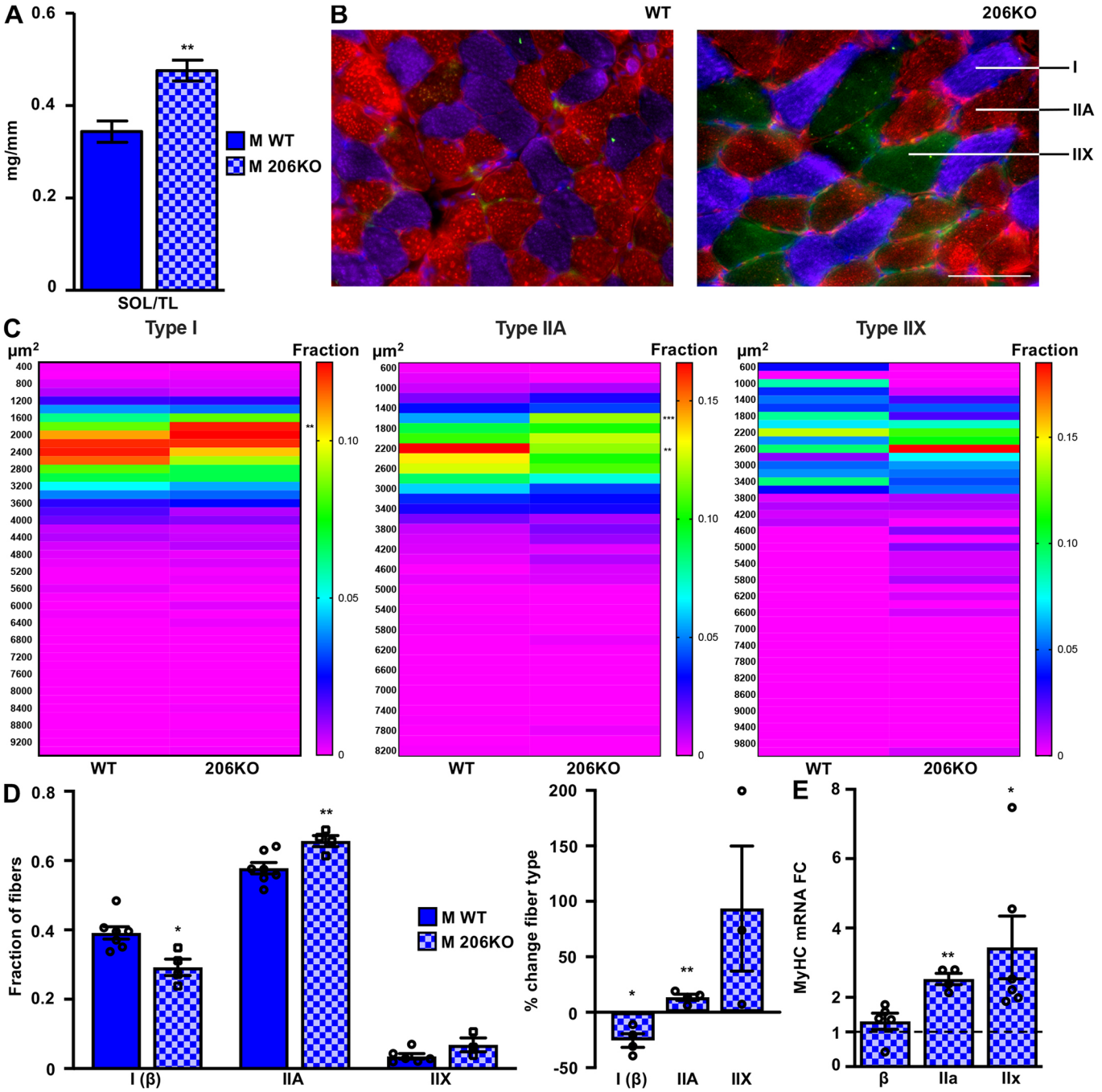

Fig. 3. miR-206 knockout increases male soleus mass and the proportion of fast fibers while slow fibers decrease. (A) SOL mass is higher in 206KO male (M) mice. Muscle mass normalized to tibia length (TL) is presented. Ns are 7 WT, 6 206KO; $^{**}P$=0.0019. (B) Representative MyHC and laminin-stained SOL cross-sections from WT (left) and 206KO (right) male mice. Type I (β-MyHC) fibers are purple, type IIA are red, and type IIX are green. Nuclei are revealed by DAPI staining (blue) and fiber borders by laminin staining (red). Scale bar: 100 μm. (C) In 206KO SOL, the cross-sectional area (CSA) of Type I myofibers are smaller, while those of types IIA and IIX are more variably sized and include the largest fibers. We measured CSA across entire soleus cross-sections from seven WT and four 206KO mice, and calculated the proportion of myofibers in 200 μm^2 bins. Heatmaps present average proportions of myofiber CSAs from each genotype. Two-way ANOVA indicated a significant effect from CSA bin. Asterisks indicate Sidak's post-test results. $^{**}P\leq0.01$, $^{***}P\leq0.001$ vs control. (D) Quantification of proportions of type I, IIA and IIX fibers across entire SOL cross-sections from seven WT and four 206KO male (M) mice (left panel), and the percentage change in each fiber type (right panel; 206KO vs WT). $^{*}P\leq0.05$, $^{**}P\leq0.01$ 206KO vs WT. (E) Fast MyHC mRNA levels increase in male 206KO SOL as measured by qPCR. WT levels are represented as a dashed line at y=1. The n values was 4–6 for each group. $^{*}P\leq0.05$, $^{**}P\leq0.01$ 206KO vs WT.

genetically linked miR-133b, suggesting a specialized role for miR-206 in promoting the slower female phenotype.

The miR-206 KO mouse model studied here was previously shown to have delayed muscle regeneration after cardiotoxin injury, impaired satellite cell differentiation, and delayed neuromuscular reinnervation (Liu et al., 2012; Williams et al., 2009). Curiously, a separate knockout mouse that is lacking not only miR-206 but also miR-133b and a portion of the muscle regulatory long noncoding RNA linc-MD1 (including the sequence encoding a miR-133 sponge) displays no overt phenotype at baseline, after acute muscle

Journal of Cell Science (2020) 133, jcs243162. doi:10.1242/jcs.243162

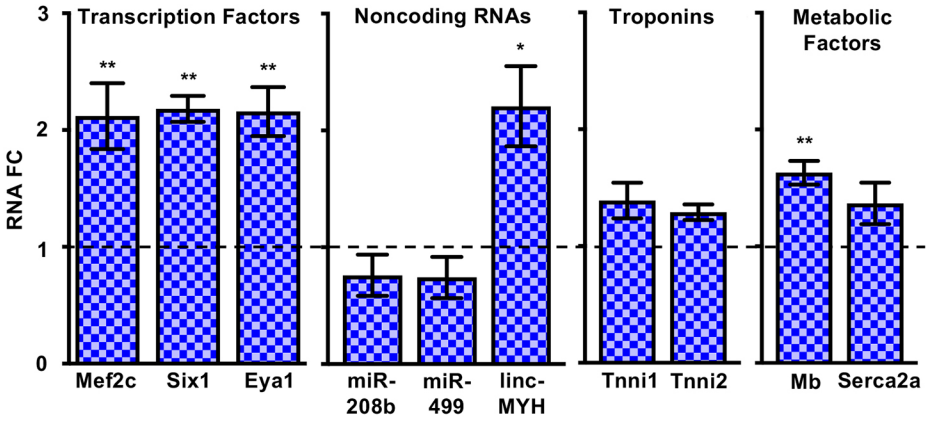

Fig. 4. The gene expression signature of the miR-206 KO soleus shifts towards fast oxidative. We measured mRNA levels of genes from diverse functional categories in the SOL by qPCR. WT levels are represented as a dashed line at y=1. The n value was 5–6 male mice per group. *P≤0.05, **P≤0.01 indicate significant differences as assessed by a Student's t-test. 206KO vs WT. Error bars show s.e.m.

injury, or in the context of muscular dystrophy (Boettger et al., 2014). However, miR-206 and miR-133 family members have been shown to play opposing roles, where the former is pro-differentiation and anti-proliferative while the latter is pro-proliferative (Chen et al., 2006; Kim et al., 2006). Moreover, double knockout of miR-133 family members miR-133a-1 and miR-133a-2 (which, collectively, differ only at the terminal 3′ position and so are presumed to target overlapping sets of transcripts) results in an increase in oxidative myofibers (Liu et al., 2011). This also supports opposing roles for miR-206 and the miR-133 family when considered with the increased proportion of fast fiber types in male 206KO SOL that we observed (Fig. 3), potentially complicating interpretation of the miR-206/miR-133b double-knockout (dKO) mouse. Supporting these observations, in Fig. 4 we show higher levels of the key fast muscle transcription factors *Six1* and *Eya1* (Grifone et al., 2004) as well as the fast-associated lncRNA linc-MYH, which is encoded in the fast MyHC genomic locus, shares a Six1/Eya1-dependent enhancer with these MyHCs and promotes fast-type gene expression (Sakakibara et al., 2014). The *Six1* 3′ UTR harbors a predicted target site for another slow muscle-specific miRNA family, miR-208/499 (TargetScan.org). Transgenic miR-499 overexpression has been shown to convert all fast fibers in the mouse SOL into slow fibers (van Rooij et al., 2009). We did not observe differential expression of either miRNA in the miR-206 KO SOL, suggesting that miR-206 could be acting downstream of miR-499 and miR-208b in promoting the slow fiber program. We also saw increased *Mef2c* and myoglobin mRNA levels in the miR-206 KO SOL (Fig. 4), which may initially seem to contradict a fast-type phenotypic switch as expression of these genes is associated with an oxidative profile. However, a recent gene expression analysis of single SOL myofibers revealed that fast oxidative fibers (types IIa and IIx) are characterized by a stronger mitochondrial and electron transport chain signature than Type I, which is consistent with our overall change in gene expression and fiber type profiles (Chemello et al., 2019). In recently published work, a mouse in which miR-206 and both miR-1a loci were knocked out resulted in partial embryonic lethality, but miR-206 single KO mice and two surviving triple KO (tKO) individuals exhibited decreased physical performance, which was supported by impaired mitochondrial function in a tKO cell culture model (Przanowska et al., 2020). Although slow skeletal muscles were not examined in that study, it would be interesting to perform a metabolic analysis of slow oxidative muscles in single, double and triple miR-1/206 family KO mice.

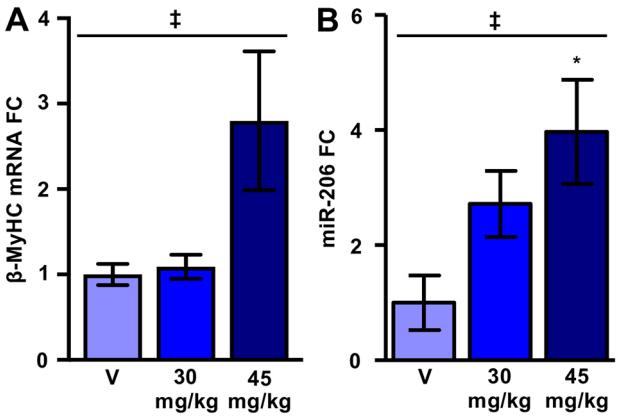

Fig. 5. Increased miR-206 expression correlates with pathological increases in slow MyHC expression in the LV. (A,B) A dose-dependent increase in β-MyHC mRNA (A) and miR-206 (B) levels in the male LV was seen with isoproterenol treatment (30 mg kg^{-1} and 45 mg kg^{-1}). We measured RNA expression by qPCR. n values are 6 for vehicle (V) and 8 for both treatments. One-way ANOVA indicated significant treatment effects for both β-MyHC and miR-206 (line with ‡). Asterisks indicate Bonferroni post-test results. *P≤0.05 vs V. Error bars show s.e.m.

miR-206 has been well-studied in the context of the early stages of myogenesis, particularly in immortalized and primary myoblast cell culture models where it inhibits proliferation and promotes the transition to differentiation by targeting transcripts such as *Pola1*, *Pax7* and *Pax3* (reviewed in McCarthy, 2008; Mitchelson, 2015). Although the targeting network through which it enforces a slow muscle phenotype is not yet clear, it notably targets the class II histone deacetylase (HDAC) *Hdac4* through translational inhibition (Williams et al., 2009; Winbanks et al., 2011). Hdac4 inhibits slow muscle gene expression and, when knocked out in mice along with other class II HDACs, results in an increased proportion of type I myofibers (Potthoff et al., 2007). This targeting relationship was established in the same miR-206 KO mice studied here when they were examined in the context of ALS (Williams et al., 2009). Interestingly, certain targets, such as *Pax7* and *Pax3*, are subject to alternative polyadenylation in different muscles, leading to different 3′ UTR sequences with differential presentation of miR-206 target sites. Thus the miR-206 targeting network is complex and will need to be considered through the lens of different muscle groups (Boutet et al., 2012; de Morree et al., 2019).

In the heart, we also found that miR-206 promotes a slow phenotype. Although adult rodents express very little β-MyHC in the ventricles, these levels are not inconsequential, and there are distinct regions where β-MyHC predominates (Krenz et al., 2007). It would be interesting to determine whether miR-206 follows the

Journal of Cell Science (2020) 133, jcs243162. doi:10.1242/jcs.243162

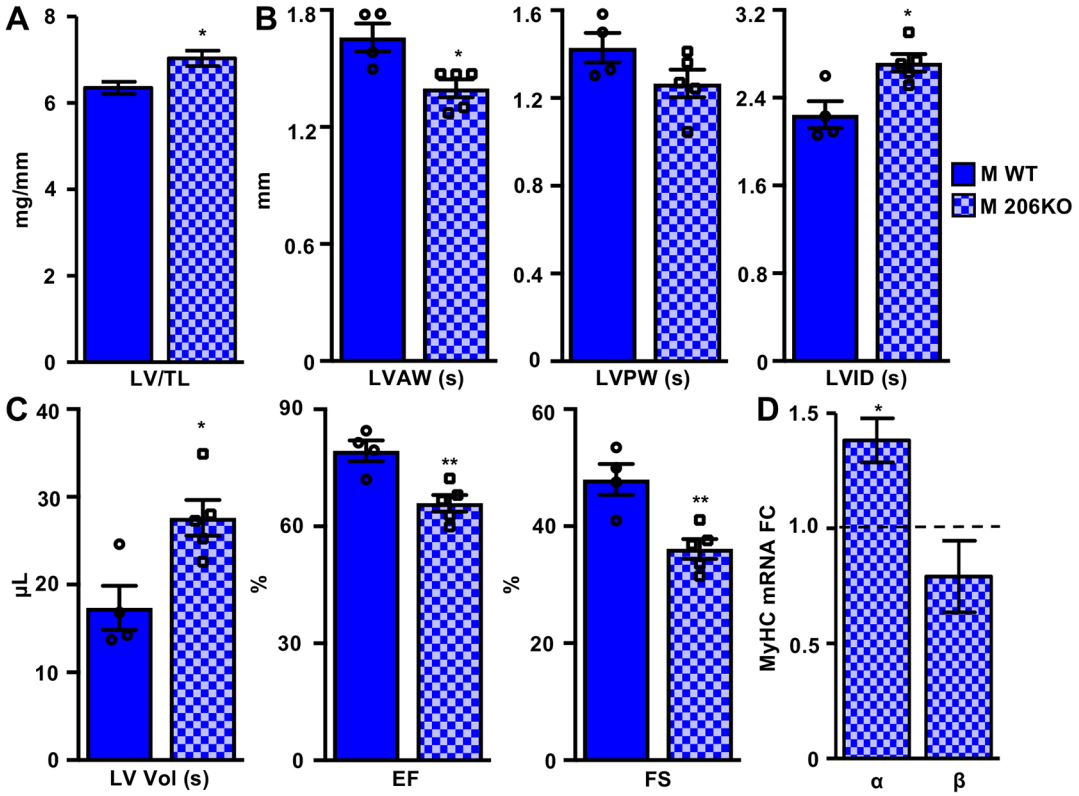

Fig. 6. miR-206 knockout results in cardiac dilation and systolic dysfunction. (A) Left ventricle (LV) mass normalized to tibia length (TL) is higher in 206KO males (M) compared to WT. *n* values are 7 for WT and 6 for 206KO. **P*≤0.05 vs WT. (B,C) M-mode echocardiographic measurements (C) and calculations (D) indicate LV dilation and systolic dysfunction in male 206KO mice. We measured LV anterior wall (LVAW) thinning with no change in LV posterior wall (LVPW), increased LV interior diameter at systole (LVID) and increased LV volume at systole (LV Vol). Both ejection fraction (EF) and fractional shortening (FS) decreased. *n* values are 4 for WT and 5 for 206KO. **P*≤0.05, ***P*≤0.01 206KO vs WT. (D) mRNA corresponding to the faster cardiac α-MyHC increases while the slower β-MyHC decreases in male 206KO LV compared to WT as measured by qPCR. WT levels are represented as a dashed line at *y*=1. *n* values are 5-6 per group. Student's *t*-test indicated a significant difference between genotypes. **P*≤0.05 206KO vs WT. Error bars show s.e.m.

cardiac β-MyHC expression pattern. In addition, the α-MyHC:β-MyHC ratio is strictly regulated. Interestingly, β-MyHC expression is reportedly 4-fold higher in the left ventricles of sexually mature female mice compared to males, and this difference is hormone dependent (Patrizio et al., 2013). We have also previously reported that isolated female rat cardiomyocytes are slower to reach both peak shortening and relaxation (Trexler et al., 2017). These observations are consistent with our comparison of female and male TA muscle. As miR-206 levels are very low in the healthy ventricle, we could not reliably compare male and female expression levels. However, we and others have detected miR-206 in primary isolated rat ventricular myocytes (Yang et al., 2015). We found 5-fold higher expression level in adult rat ventricular myocytes compared to neonatal rat ventricular myocytes (NRVMs) and 15-fold higher expression in NRVMs compared to neonatal rat ventricular fibroblasts, supporting the notion that cardiac miR-206 is expressed specifically in myocytes (data not shown).

If miR-206 is also an enforcer of slow gene expression in the heart, we predict that: (1) in the absence of miR-206, the heart would shift towards a faster phenotype, and (2) miR-206 expression would increase in pathological conditions when the heart shifts towards a slower phenotype. Accordingly, we observed a significant increase in α-MyHC expression and a downward trend in β-MyHC expression in miR-206 KO LVs (Fig. 6D). Supporting the assertion that the small amount of β-MyHC that is expressed in the mouse heart is still critical for normal function, we observed ventricular dilation and systolic dysfunction in miR-206 KO mice (Fig. 6B,C). As in skeletal muscle, this is a male-specific phenomenon, the mechanistic basis for which is an intriguing area for future investigation. Interestingly, transgenic mice overexpressing miR-206 experience cardiac hypertrophy, which, combined with our knockout data, suggests the importance of maintaining miR-206 levels within a narrow range at baseline (Yang et al., 2015). However, miR-1 levels also increased in these transgenic miR-206 mice, and miR-1 overexpression in the heart is known to be detrimental (Zhao et al., 2005).

In support of our second prediction, we observed a dose-dependent increase in miR-206 expression in the left ventricles of wild-type mice treated with the β-adrenergic receptor agonist, isoproterenol. Several reports have also noted increased miR-206 expression after MI in multiple animal models (Dong et al., 2009; Limana et al., 2011; Shan et al., 2009). Both MI and β-adrenergic stimulation are associated with increased β-MyHC expression at the expense of the faster α-MyHC (Harada et al., 1999; Fig. 5A). This may be a compensatory acute stress-adaptation mechanism as β-MyHC is a more energetically efficient motor. This is supported by the finding that adenoviral-mediated overexpression of miR-206 in rat hearts protects from ischemia–reperfusion injury (Zhai et al., 2017). We speculate that miR-206 KO mice would be less able to adapt to cardiac stress as they may not properly induce β-MyHC. Indeed, transgenic mice expressing a miR-206 sponge develop larger infarcts after ischemia–reperfusion injury than wild-type animals (Yang et al., 2015). As this miRNA sponge may also inhibit

Journal of Cell Science (2020) 133, jcs243162. doi:10.1242/jcs.243162

miR-1, which is the most abundant cardiac miRNA, it will be important to examine the response of miR-206 KO mice to cardiac injury in the future.

Collectively, our data indicate that miR-206 enforces slow muscle gene expression, which ultimately tunes both skeletal and cardiac muscle performance. Moreover, the consistent protective role of miR-206 under pathological conditions in both tissues makes it an attractive target for RNA-based therapeutics.

MATERIALS AND METHODS

Cloning and mutagenesis

The minimal promoter (minTATA) and MyoG enhancer firefly luciferase reporter gene constructs were previously described (Cheung et al., 2007). We cloned the miR-206 enhancer (GRCm38/mm10 chr1:20,678,053-20,678,259) in the same manner as described for MyoG. We generated E-box point mutations (CANNTG→CANNTA) with the QuikChange II site-directed mutagenesis kit (Agilent, 200523, Santa Clara, CA) as per the manufacturer's instructions. We verified all clones by Sanger sequencing. MRF expression constructs were a kind gift from Dr Xuedong Liu (University of Colorado Boulder, Boulder, CO). Primer sequences are listed in Table S1.

Cell culture and transfection

We grew C2C12 myoblasts (a gift from Dr Helen Blau, Stanford University, Stanford, CA) in growth medium [GM; high-glucose DMEM (Invitrogen, 11960069, Waltham, MA) supplemented with 20% fetal bovine serum, 2 mM L-glutamine, 100 U ml^{-1} penicillin and 100 µg ml^{-1} streptomycin, and 1 mM sodium pyruvate]. We differentiated them to myotubes by changing the medium to differentiation medium [DM; high-glucose DMEM supplemented with 5% adult horse serum, 2 mM L-glutamine, 100 U ml^{-1} penicillin and 100 µg ml^{-1} streptomycin, and 1 mM sodium pyruvate]. When differentiating, we refreshed DM every day to prevent medium acidification. We grew 10T1/2 cells (ATCC, Manassas, VA) in GM but with 10% FBS. For luciferase assays, we plated cells in triplicate in six-well dishes at a density of 50,000 cells/well (C2C12) or 100,000 cells/well (10T1/2) 24 h before transfection. We repeated each experiment at least twice with independent batches of cells. We routinely tested cells for mycoplasma contamination. We transfected with *Trans*IT-LT1 (Mirus Bio, MIR 2305, Madison, WI) according to the manufacturer's instructions. We co-transfected all firefly luciferase constructs with pRL-TK as a control. When differentiating C2C12 myotubes, we collected day 0 time points at 24 h post-transfection and initiated differentiation at the same time for later time points. We collected 10T1/2 cells at 24 h post transfection. At harvest, we washed cells twice with phosphate-buffered saline (PBS) solution, and stored them in an ultralow freezer in order to process all time points together at the end of the experiment.

Luciferase assays

We used a Dual-Luciferase Reporter Assay System (Promega, E1960, Madison, WI) according to the manufacturer's instructions with a Turner Designs TD-20/20 luminometer. Briefly, we lysed frozen cells in 1× passive lysis buffer and measured reporter gene activities first in LARII reagent (firefly luciferase) and second in Stop & Glo reagent (*Renilla* luciferase). Read times for both were 10 s. We compared ratios of Renilla:firefly luminescence.

Mice

The University of Colorado Boulder and Colorado State University Institutional Animal Care and Use Committees approved all animal work under protocols 1301.05, 1002.07, and 1002.08. Mice (*Mus musculus*) were 4-month-old wild-type C57Bl/6J (Jackson Laboratories, 000664, Sacramento, CA), 6–7-month-old miR-206 KO (a kind gift from Dr Eric Olson, University of Texas Southwestern Medical Center and described in Williams et al., 2009), and 4-month-old *mdx4cv* (a kind gift from Dr Bradley Olwin, University of Colorado Boulder). Aromatase knockout (ArKO) mice were 4 months old, as this age precedes the age-dependent increase in testosterone observed in the ArKO females (Haines et al., 2012). Mice were housed in standard temperature and humidity-controlled environments with a 12-h-light–12-h-dark cycle and offered food and water *ad libitum*. We euthanized mice by cervical dislocation under inhaled isoflurane. We excised and flash froze all tissues used for molecular analyses in liquid nitrogen. For muscles used for sectioning and staining, we excised and embedded tissues in OCT compound and then froze them in melting isopentane chilled with liquid nitrogen.

We used animals from multiple litters to achieve the pre-determined group sizes and always included littermates. We randomly allocated animals to experimental groups within a genotype. For genetically modified animals, we bred heterozygotes together to ensure littermates of both WT and genetically modified genotypes. Within a strain, we co-housed animals of the same sex to provide equivalent environments between genotypes.

Cage activity

To model endurance exercise, we provided a cage wheel to mice and allowed them to run voluntarily as previously described (Allen et al., 2001). To model muscle unloading, we performed hindlimb suspension as previously described (Allen et al., 2009). We suspended the tail at a 30° angle by taping it to a plastic dowel attached to a swivel apparatus. The forelimbs were still in contact with the cage bottom. We attached the suspension apparatus to a guide wire so mice were able to access all areas of the cage. We euthanized mice and harvested tissues 3, 7 or 14 days after initiating exercise or hindlimb suspension. We compared samples from exercised or hindlimb suspension mice to age-matched normal cage activity controls.

Isoproterenol treatment

We chronically administered isoproterenol in 1 µM ascorbic acid diluted in sterile saline to C57Bl/6J wild-type male mice via subcutaneous implantation of a miniosmotic pump (model 2001; Alzet, Cupertino, CA). The pumps delivered isoproterenol at a dose of 30 or 45 mg kg^{-1} body weight per day. Vehicle control pumps contained 1 µM ascorbic acid diluted in sterile saline. We euthanized mice as described above 7 days after pump implantation.

$BaCl_2$ injury

We injured the TA or gastrocnemius with barium chloride as previously described (Guess et al., 2013). Briefly, we anesthetized wild-type C57Bl/6J male mice with 1–4% inhaled isoflurane and shaved the right hind limb. We cleaned the shaved area with 70% ethanol and used a 27-gauge insulin syringe to inject the muscle with 50 µl of 1.2% $BaCl_2$ dissolved in normal saline. We monitored mice for adverse effects while they recovered on a 37°C heat block.

Echocardiography

We performed M-mode transthoracic echocardiography as previously described (Haines et al., 2012). Briefly, we mildly sedated each animal immediately before imaging with 2% inhaled isoflurane. We used a rodent-specific echocardiography machine (Visualsonics, Toronto, Canada) and a 15 MHz linear array probe to image at the midpapillary muscle level. We analyzed images with Echo-Pack software (GE Vingmed, Horten, Norway). Heart rate was the same in all groups of 206KO and WT mice (Fig. S5B). Each measurement per animal represents the average of three consecutive cardiac cycles.

Hydrodynamic limb vein injection and *in vivo* imaging

We performed hydrodynamic limb vein (HLV) injections and subsequent *in vivo* reporter gene activity imaging as previously described (Guess et al., 2013). Briefly, we co-injected the miR-206 enhancer-driven luciferase plasmid or the basal promoter-only (minTATA) control plasmid with the normalization construct p-mKate, which expresses a far red fluorescent protein from a constitutively active promoter. To ensure the plasmids remained only in the hindlimb that was injected but were widely distributed across muscle groups in that limb, we applied a tourniquet around the upper thigh of the anesthetized mouse to restrict blood flow for 1 to 2 min and then injected a large volume {determined by [1+((body weight in grams−25)/25)×1/2] ml} at a rate of 7 ml min^{-1} with a syringe pump. This method is highly effective for delivering plasmid DNA to muscles with minimal damage (Hagstrom et al., 2004).

Human biopsies

Human DMD (kindly provided by Dr Eric Hoffman of George Washington University) and healthy control vastus lateralis (VL) biopsy samples were previously described (Guess et al., 2015). The University of Colorado Human Research Institutional Review Board (IRB) considered the DMD samples exempt from approval according to the University of Colorado Human Research IRB guidelines and approved collection of control biopsies under IRB Protocol 0402.11, August 2002.

Sectioning and immunostaining

We cut 10 µm sections with a cryostat chilled to −20°C from the mid-belly of the soleus and immunostained with standard techniques. Primary antibodies against different MyHC isoforms were produced in-house from hybridoma cell lines purchased from Developmental Studies Hybridoma Bank, Iowa City, IA [MyHC IIa (SC-71; used at 1:2 dilution), MyHC IIx (6H1; used at 1:5 dilution), and β-MyHC (BA-D5; used at 1:50 dilution)]. We used 1:100 dilutions of isotype-specific secondary antibodies [FITC-goat α-mouse IgM (Jackson 115-095-075), Alexa Fluor 568-goat α-mouse IgG1 (Invitrogen A-21124), and Alexa Fluor 647-goat α-mouse IgG2b (Jackson 15-605-207)]. Laminin primary antibody was from Sigma (L-9393, St Louis, MO; used at 1:100 dilution) and secondary was TR-donkey α-rabbit (Jackson 711-075-152; used at 1:100 dilution). We stained DNA with DAPI. We collected all images on a Nikon TE2000 inverted fluorescent microscope with a 20× objective connected to a Nikon DS-QiMc-U3 camera controlled through the NIS-Elements AR software version 4.00.03. We kept exposure times for a given channel constant for all slides. We processed raw images with the Image5D plugin in ImageJ using the same settings for a given channel across all images.

Fiber typing

In ImageJ, we manually counted fiber types across entire soleus sections (7 WT and 4 206KO mice) based on MyHC immunostaining. This analysis was double blinded: before analysis, we provided images with non-descriptive, numbered labels to an investigator not involved in the study who then relabeled them and returned them for analysis. After scoring fiber types for each section, we asked for the labeling key in order to reveal genotypes.

Cross-sectional area measurements

We manually measured myofiber cross-sectional area across entire laminin- and MyHC-stained soleus sections (seven WT and four 206KO mice; 4924 total fibers) using ImageJ. This analysis was also double blinded as described in the fiber typing section.

RNA isolation and qPCR analysis

We isolated total RNA with TRI Reagent (MRC, TR 118, Cincinnati, OH) according to the manufacturer's protocol. We homogenized frozen tissue samples directly into ice cold TRI reagent using a dispersion tool (IKA, T10 Basic S1, Wilmington, NC). For pri-miR-206 analysis, we DNase treated the RNA (TURBO DNA-free kit; Thermo Fisher, AM1907, Waltham, MA) as the qPCR primers could not be intron-spanning. We performed all qPCR on an ABI 7500 Fast Real-Time PCR System. We assessed miRNA expression by TaqMan-based qPCR (Thermo Fisher, Part Number 4427975). We reverse transcribed miRNAs with a TaqMan MicroRNA Reverse Transcription Kit (Thermo Fisher, 4366596) and performed qPCR with TaqMan Universal PCR Master Mix, No AmpErase UNG (Thermo Fisher, 4324018), all according to the manufacturer's instructions. We used the $\Delta\Delta C_T$ method to analyze relative expression. We normalized all mouse miRNAs to sno202 expression levels and human miR-206 to U6 RNA. We measured mRNA expression with SYBR Green-based qPCR. All primer sequences are listed in Table S1. We reverse transcribed total RNA with random hexamer primers using the Superscript II Reverse Transcriptase kit (Thermo Fisher, 18064-022). We performed qPCR with SYBR Green PCR Master Mix (Thermo Fisher, 4312704) according to the manufacturer's instructions. We measured relative expression with the Pfaffl standard curve method. In regenerating TA (Fig. 2D, Fig. S1D,E) and isoproterenol-treated heart samples (Fig. 5A; Fig. S4D), we normalized RNA levels to 18S rRNA. In 206KO and WT soleus samples (Figs 3 and 4), we normalized mRNA levels to *Acta1*. In the 206KO and WT heart samples (Fig. 6D; Figs S5C and S6B), we normalized mRNA levels to *Gapdh*. Per animal, each data point is the average of technical duplicates.

Graphing and statistical analysis

We graphed and analyzed all data for statistical significance with GraphPad Prism. We analyzed simple two-group comparisons with a Student's *t*-test. We analyzed multi-group comparisons with ANOVA followed by a Bonferroni post-test or Sidak's multiple comparisons test in the case of CSA analysis (Fig. 3C). $P<0.05$ was taken as the significance threshold. Other statistical cutoffs are as noted in the figure legends. Data are presented as means with error bars representing the s.e.m. For experiments in which any group size was smaller than five, we present individual points as well as the mean. The *n* values for each experimental group are noted in the figure legends. To determine sample size for animal experiments, we performed a power analysis based on our preliminary data using G*Power (Faul et al., 2007). We assessed the presence of outliers by determining interquartile ranges and excluded data points more than 1.5× below the first or above the third quartile.

Acknowledgements

We thank Dr Eric Olson (UT-Southwestern) for generously providing the miR-206 KO mice. We also thank Amy Perry for performing echocardiography measurements, Darrian Bugg, Chris Haines and Dr Alberto Rossi for technical assistance, Drs Emily Pugach, Christa Trexler and Massimo Buvoli for valuable conversations and insight, Dr Sarah Lehman for critical reading and feedback, and the University of Colorado Boulder BioFrontiers Advanced Light Microscopy Core facility for support with fluorescence microscopy.

Competing interests

The authors declare no competing or financial interests.

Author contributions

Conceptualization: K.K.B., B.C.H., A.K.P., L.A.L.; Methodology: K.K.B., M.G.G., B.C.H., A.K.P.; Validation: K.K.B.; Formal analysis: K.K.B., M.G., A.K.P.; Investigation: K.K.B., M.G.G., B.C.H., M.M.P., A.K.P.; Resources: K.K.B.; Data curation: K.K.B.; Writing - original draft: K.K.B.; Writing - review & editing: K.K.B., M.G.G., B.C.H., M.M.P., A.K.P., L.A.L.; Visualization: K.K.B.; Supervision: L.A.L.; Project administration: L.A.L.; Funding acquisition: K.K.B., M.G.G., B.C.H., L.A.L.

Funding

This work was supported by National Institutes of Health (GM29090 to L.A.L.), K.K.B. was supported by National Institutes of Health post-doctoral training grant 2T32HL007822-11A2 and American Heart Association post-doctoral fellowship 13POST14410014, M.G.G. was supported by National Institutes of Health pre-doctoral training grant 5T32GM007135-36, and B.C.H. was supported by National Institutes of Health Research Scientist Development Award K01AR055676. Deposited in PMC for release after 12 months.

Supplementary information

Supplementary information available online at
https://jcs.biologists.org/lookup/doi/10.1242/jcs.243162.supplemental

Peer review history

The peer review history is available online at
https://jcs.biologists.org/lookup/doi/10.1242/jcs.243162.reviewer-comments.pdf

References

Adams, B. D., Furneaux, H. and White, B. A. (2007). The micro-ribonucleic acid (miRNA) miR-206 targets the human estrogen receptor-α (ERα) and represses ERα messenger RNA and protein expression in breast cancer cell lines. *Mol. Endocrinol.* **21**, 1132-1147. doi:10.1210/me.2007-0022

Allen, D. L., Harrison, B. C., Maass, A., Bell, M. L., Byrnes, W. C. and Leinwand, L. A. (2001). Cardiac and skeletal muscle adaptations to voluntary wheel running in the mouse. *J. Appl. Physiol.* **90**, 1900-1908. doi:10.1152/jappl.2001.90.5.1900

Allen, D. L., Bandstra, E. R., Harrison, B. C., Thorng, S., Stodieck, L. S., Kostenuik, P. J., Morony, S., Lacey, D. L., Hammond, T. G., Leinwand, L. L. et al. (2009). Effects of spaceflight on murine skeletal muscle gene expression. *J. Appl. Physiol.* **106**, 582-595. doi:10.1152/japplphysiol.90780.2008

Andersen, P. and Henriksson, J. (1977). Training induced changes in the subgroups of human type II skeletal muscle fibres. *Acta Physiol. Scand.* **99**, 123-125. doi:10.1111/j.1748-1716.1977.tb10361.x

Boettger, T., Wüst, S., Nolte, H. and Braun, T. (2014). The miR-206/133b cluster is dispensable for development, survival and regeneration of skeletal muscle. *Skelet. Muscle* **4**, 23. doi:10.1186/s13395-014-0023-5

Boutet, S. C., Cheung, T. H., Quach, N. L., Liu, L., Prescott, S. L., Edalati, A., Iori, K. and Rando, T. A. (2012). Alternative polyadenylation mediates microRNA regulation of muscle stem cell function. *Cell Stem Cell* **10**, 327-336. doi:10.1016/j.stem.2012.01.017

Caiozzo, V. J., Baker, M. J. and Baldwin, K. M. (1998). Novel transitions in MHC isoforms: separate and combined effects of thyroid hormone and mechanical unloading. *J. Appl. Physiol.* **85**, 2237-2248. doi:10.1152/jappl.1998.85.6.2237

Chemello, F., Grespi, F., Zulian, A., Cancellara, P., Hebert-Chatelain, E., Martini, P., Bean, C., Alessio, E., Buson, L., Bazzega, M. et al. (2019). Transcriptomic analysis of single isolated myofibers identifies miR-27a-3p and miR-142-3p as regulators of metabolism in skeletal muscle. *Cell Rep.* **26**, 3784-3797.e8. doi:10.1016/j.celrep.2019.02.105

Chen, J.-F., Mandel, E. M., Thomson, J. M., Wu, Q., Callis, T. E., Hammond, S. M., Conlon, F. L. and Wang, D.-Z. (2006). The role of microRNA-1 and microRNA-133 in skeletal muscle proliferation and differentiation. *Nat. Genet.* **38**, 228-233. doi:10.1038/ng1725

Cheung, T. H., Barthel, K. K. B., Kwan, Y. L. and Liu, X. (2007). Identifying pattern-defined regulatory islands in mammalian genomes. *Proc. Natl. Acad. Sci. USA* **104**, 10116-10121. doi:10.1073/pnas.0704028104

Ciciliot, S. and Schiaffino, S. (2010). Regeneration of mammalian skeletal muscle: basic mechanisms and clinical implications. *Curr. Pharm. Des.* **16**, 906-914. doi:10.2174/138161210790883453

de Morree, A., Klein, J. D. D., Gan, Q., Farup, J., Urtasun, A., Kanugovi, A., Bilen, B., van Velthoven, C. T. J., Quarta, M. and Rando, T. A. (2019). Alternative polyadenylation of Pax3 controls muscle stem cell fate and muscle function. *Science* **366**, 734-738. doi:10.1126/science.aax1694

Dong, S., Cheng, Y., Yang, J., Li, J., Liu, X., Wang, X., Wang, D., Krall, T. J., Delphin, E. S. and Zhang, C. (2009). MicroRNA expression signature and the role of MicroRNA-21 in the early phase of acute myocardial infarction. *J. Biol. Chem.* **284**, 29514-29525. doi:10.1074/jbc.M109.027896

Faul, F., Erdfelder, E., Lang, A.G. and Buchner, A. (2007). G*Power 3: a flexible statistical power analysis program for the social, behavioral, and biomedical sciences. *Behav. Res. Methods* **39**, 175-191. doi:10.3758/bf03193146

Gokhin, D. S., Ward, S. R., Bremner, S. N. and Lieber, R. L. (2008). Quantitative analysis of neonatal skeletal muscle functional improvement in the mouse. *J. Exp. Biol.* **211**, 837-843. doi:10.1242/jeb.014340

Grifone, R., Laclef, C., Spitz, F., Lopez, S., Demignon, J., Guidotti, J.-E., Kawakami, K., Xu, P.-X., Kelly, R., Petrof, B. J. et al. (2004). Six1 and Eya1 expression can reprogram adult muscle from the slow-twitch phenotype into the fast-twitch phenotype. *Mol. Cell. Biol.* **24**, 6253-6267. doi:10.1128/MCB.24.14.6253-6267.2004

Guess, M. G., Barthel, K. K. B., Pugach, E. K. and Leinwand, L. A. (2013). Measuring microRNA reporter activity in skeletal muscle using hydrodynamic limb vein injection of plasmid DNA combined with in vivo imaging. *Skelet. Muscle* **3**, 19. doi:10.1186/2044-5040-3-19

Guess, M. G., Barthel, K. K. B., Harrison, B. C. and Leinwand, L. A. (2015). miR-30 family microRNAs regulate myogenic differentiation and provide negative feedback on the microRNA pathway. *PLoS ONE* **10**, e0118229. doi:10.1371/journal.pone.0118229

Hagstrom, J. E., Hegge, J., Zhang, G., Noble, M., Budker, V., Lewis, D. L., Herweijer, H. and Wolff, J. A. (2004). A facile nonviral method for delivering genes and siRNAs to skeletal muscle of mammalian limbs. *Mol. Ther.* **10**, 386-398. doi:10.1016/j.ymthe.2004.05.004

Haines, C. D., Harvey, P. A. and Leinwand, L. A. (2012). Estrogens mediate cardiac hypertrophy in a stimulus-dependent manner. *Endocrinology* **153**, 4480-4490. doi:10.1210/en.2012-1353

Haizlip, K. M., Harrison, B. C. and Leinwand, L. A. (2015). Sex-based differences in skeletal muscle kinetics and fiber-type composition. *Physiology* **30**, 30-39. doi:10.1152/physiol.00024.2014

Hamrick, M. W., Herberg, S., Arounleut, P., He, H.-Z., Shiver, A., Qi, R.-Q., Zhou, L., Isales, C. M. and Mi, Q. S. (2010). The adipokine leptin increases skeletal muscle mass and significantly alters skeletal muscle miRNA expression profile in aged mice. *Biochem. Biophys. Res. Commun.* **400**, 379-383. doi:10.1016/j.bbrc.2010.08.079

Harada, K., Sugaya, T., Murakami, K., Yazaki, Y. and Komuro, I. (1999). Angiotensin II type 1A receptor knockout mice display less left ventricular remodeling and improved survival after myocardial infarction. *Circulation* **100**, 2093-2099. doi:10.1161/01.CIR.100.20.2093

Harrison, B. C., Allen, D. L., Girten, B., Stodieck, L. S., Kostenuik, P. J., Bateman, T. A., Morony, S., Lacey, D. and Leinwand, L. A. (2003). Skeletal muscle adaptations to microgravity exposure in the mouse. *J. Appl. Physiol.* **95**, 2462-2470. doi:10.1152/japplphysiol.00603.2003

Hoyer, K., Krenz, M., Robbins, J. and Ingwall, J. S. (2007). Shifts in the myosin heavy chain isozymes in the mouse heart result in increased energy efficiency. *J. Mol. Cell. Cardiol.* **42**, 214-221. doi:10.1016/j.yjmcc.2006.08.116

Izumo, S., Lompré, A. M., Matsuoka, R., Koren, G., Schwartz, K., Nadal-Ginard, B. and Mahdavi, V. (1987). Myosin heavy chain messenger RNA and protein isoform transitions during cardiac hypertrophy. Interaction between hemodynamic and thyroid hormone-induced signals. *J. Clin. Invest.* **79**, 970-977. doi:10.1172/JCI112908

Janssen, I., Heymsfield, S. B., Wang, Z. M. and Ross, R. (2000). Skeletal muscle mass and distribution in 468 men and women aged 18-88 yr. *J. Appl. Physiol.* **89**, 81-88. doi:10.1152/jappl.2000.89.1.81

Kim, H. K., Lee, Y. S., Sivaprasad, U., Malhotra, A. and Dutta, A. (2006). Muscle-specific microRNA miR-206 promotes muscle differentiation. *J. Cell Biol.* **174**, 677-687. doi:10.1083/jcb.200603008

Kim, J. Y., Park, Y.-K., Lee, K.-P., Lee, S.-M., Kang, T.-W., Kim, H.-J., Dho, S. H., Kim, S.-Y. and Kwon, K.-S. (2014). Genome-wide profiling of the microRNA-mRNA regulatory network in skeletal muscle with aging. *Aging (Albany. NY).* **6**, 524-544. doi:10.18632/aging.100677

Krenz, M. and Robbins, J. (2004). Impact of beta-myosin heavy chain expression on cardiac function during stress. *J. Am. Coll. Cardiol.* **44**, 2390-2397. doi:10.1016/j.jacc.2004.09.044

Krenz, M., Sadayappan, S., Osinska, H. E., Henry, J. A., Beck, S., Warshaw, D. M. and Robbins, J. (2007). Distribution and structure-function relationship of myosin heavy chain isoforms in the adult mouse heart. *J. Biol. Chem.* **282**, 24057-24064. doi:10.1074/jbc.M704574200

Limana, F., Esposito, G., D'Arcangelo, D., Di Carlo, A., Romani, S., Melillo, G., Mangoni, A., Bertolami, C., Pompilio, G., Germani, A. et al. (2011). HMGB1 attenuates cardiac remodelling in the failing heart via enhanced cardiac regeneration and miR-206-mediated inhibition of TIMP-3. *PLoS ONE* **6**, e19845. doi:10.1371/journal.pone.0019845

Liu, N., Bezprozvannaya, S., Shelton, J. M., Frisard, M. I., Hulver, M. W., McMillan, R. P., Wu, Y., Voelker, K. A., Grange, R. W., Richardson, J. A. et al. (2011). Mice lacking microRNA 133a develop dynamin 2-dependent centronuclear myopathy. *J. Clin. Invest.* **121**, 3258-3268. doi:10.1172/JCI46267

Liu, N., Williams, A. H., Maxeiner, J. M., Bezprozvannaya, S., Shelton, J. M., Richardson, J. A., Bassel-Duby, R. and Olson, E. N. (2012). microRNA-206 promotes skeletal muscle regeneration and delays progression of Duchenne muscular dystrophy in mice. *J. Clin. Invest.* **122**, 2054-2065. doi:10.1172/JCI62656

Ma, G., Wang, Y., Li, Y., Cui, L., Zhao, Y., Zhao, B. and Li, K. (2015). MiR-206, a key modulator of skeletal muscle development and disease. *Int. J. Biol. Sci.* **11**, 345-352. doi:10.7150/ijbs.10921

McCarthy, J. J. (2008). MicroRNA-206: the skeletal muscle-specific myomiR. *Biochim. Biophys. Acta Gene Regul. Mech.* **1779**, 682-691. doi:10.1016/j.bbagrm.2008.03.001

McCarthy, J. J., Fox, A. M., Tsika, G. L., Gao, L. and Tsika, R. W. (1997). β-MHC transgene expression in suspended and mechanically overloaded/suspended soleus muscle of transgenic mice. *Am. J. Physiol. Regul. Integr. Comp. Physiol.* **272**, R1552-R1561. doi:10.1152/ajpregu.1997.272.5.R1552

Mitchelson, K. R. (2015). Roles of the canonical myomiRs miR-1, -133 and -206 in cell development and disease. *World J. Biol. Chem.* **6**, 162-208. doi:10.4331/wjbc.v6.i3.162

Miyata, S., Minobe, W., Bristow, M. R. and Leinwand, L. A. (2000). Myosin heavy chain isoform expression in the failing and nonfailing human heart. *Circ. Res.* **86**, 386-390. doi:10.1161/01.RES.86.4.386

Nadal-Ginard, B. and Mahdavi, V. (1989). Molecular basis of cardiac performance. Plasticity of the myocardium generated through protein isoform switches. *J. Clin. Invest.* **84**, 1693-1700. doi:10.1172/JCI114351

Nakao, K., Minobe, W., Roden, R., Bristow, M. R. and Leinwand, L. A. (1997). Myosin heavy chain gene expression in human heart failure. *J. Clin. Invest.* **100**, 2362-2370. doi:10.1172/JCI119776

Nohata, N., Hanazawa, T., Enokida, H. and Seki, N. (2012). microRNA-1/133a and microRNA-206/133b clusters: dysregulation and functional roles in human cancers. *Oncotarget* **3**, 9-21. doi:10.18632/oncotarget.424

O'Rourke, J. R., Georges, S. A., Seay, H. R., Tapscott, S. J., McManus, M. T., Goldhamer, D. J., Swanson, M. S. and Harfe, B. D. (2007). Essential role for Dicer during skeletal muscle development. *Dev. Biol.* **311**, 359-368. doi:10.1016/j.ydbio.2007.08.032

Patrizio, M., Musumeci, M., Piccone, A., Raggi, C., Mattei, E. and Marano, G. (2013). Hormonal regulation of β-myosin heavy chain expression in the mouse left ventricle. *J. Endocrinol.* **216**, 287-296. doi:10.1530/JOE-12-0201

Pereira Sant'Ana, J. A. A., Ennion, S., Sargeant, A. J., Moorman, A. F. M. and Goldspink, G. (1997). Comparison of the molecular, antigenic and ATPase determinants of fast myosin heavy chains in rat and human: a single-fibre study. *Pflugers Arch. Eur. J. Physiol.* **435**, 151-163. doi:10.1007/s004240050495

Potthoff, M. J., Wu, H., Arnold, M. A., Shelton, J. M., Backs, J., McAnally, J., Richardson, J. A., Bassel-Duby, R. and Olson, E. N. (2007). Histone deacetylase degradation and MEF2 activation promote the formation of slow-twitch myofibers. *J. Clin. Invest.* **117**, 2459-2467. doi:10.1172/JCI31960

Przanowska, R. K., Sobierajska, E., Su, Z., Jensen, K., Przanowski, P., Nagdas, S., Kashatus, J. A., Kashatus, D. F., Bhatnagar, S., Lukens, J. R. et al. (2020). miR-206 family is important for mitochondrial and muscle function, but not essential for myogenesis in vitro. *FASEB J.* **34**, 7687-7702. doi:10.1096/fj.201902855RR

Rao, P. K., Kumar, R. M., Farkhondeh, M., Baskerville, S. and Lodish, H. F. (2006). Myogenic factors that regulate expression of muscle-specific microRNAs. *Proc. Natl. Acad. Sci. USA* **103**, 8721-8726. doi:10.1073/pnas.0602831103

Resnicow, D. I., Deacon, J. C., Warrick, H. M., Spudich, J. A. and Leinwand, L. A. (2010). Functional diversity among a family of human skeletal muscle myosin motors. *Proc. Natl. Acad. Sci. USA* **107**, 1053-1058. doi:10.1073/pnas.0913527107

Ross, A. and Leveritt, M. (2001). Long-term metabolic and skeletal muscle adaptations to short-sprint training: implications for sprint training and tapering. *Sport. Med.* **31**, 1063-1082. doi:10.2165/00007256-200131150-00003

Sadayappan, S., Gulick, J., Klevitsky, R., Lorenz, J. N., Sargent, M., Molkentin, J. D. and Robbins, J. (2009). Cardiac myosin binding protein-C phosphorylation in a β-myosin heavy chain background. *Circulation* **119**, 1253-1262. doi:10.1161/CIRCULATIONAHA.108.798983

Sakakibara, I., Santolini, M., Ferry, A., Hakim, V. and Maire, P. (2014). Six homeoproteins and a linc-RNA at the fast MYH locus lock fast myofiber terminal phenotype. *PLoS Genet.* **10**, e1004386. doi:10.1371/journal.pgen.1004386

Shan, Z.-X., Lin, Q.-X., Fu, Y.-H., Deng, C.-Y., Zhou, Z.-L., Zhu, J.-N., Liu, X.-Y., Zhang, Y.-Y., Li, Y., Lin, S.-G. et al. (2009). Upregulated expression of miR-1/miR-206 in a rat model of myocardial infarction. *Biochem. Biophys. Res. Commun.* **381**, 597-601. doi:10.1016/j.bbrc.2009.02.097

Shan, Z.-X., Lin, Q.-X., Deng, C.-Y., Zhu, J.-N., Mai, L.-P., Liu, J.-L., Fu, Y.-H., Liu, X.-Y., Li, Y.-X., Zhang, Y.-Y. et al. (2010). MiR-1/miR-206 regulate Hsp60 expression contributing to glucose-mediated apoptosis in cardiomyocytes. *FEBS Lett.* **584**, 3592-3600. doi:10.1016/j.febslet.2010.07.027

Sheng, J.J. and Jin, J.P. (2016). TNNI1, TNNI2 and TNNI3: evolution, regulation, and protein structure-function relationships. *Gene* **576**, 385-394. doi:10.1016/j.gene.2015.10.052

Sweetman, D., Goljanek, K., Rathjen, T., Oustanina, S., Braun, T., Dalmay, T. and Münsterberg, A. (2008). Specific requirements of MRFs for the expression of muscle specific microRNAs, miR-1, miR-206 and miR-133. *Dev. Biol.* **321**, 491-499. doi:10.1016/j.ydbio.2008.06.019

Taegtmeyer, H., Sen, S. and Vela, D. (2010). Return to the fetal gene program: a suggested metabolic link to gene expression in the heart. *Ann. N. Y. Acad. Sci.* **1188**, 191-198. doi:10.1111/j.1749-6632.2009.05100.x

Trexler, C. L., Odell, A. T., Jeong, M. Y., Dowell, R. D. and Leinwand, L. A. (2017). Transcriptome and functional profile of cardiac myocytes is influenced by biological sex. *Circ. Cardiovasc. Genet.* **10**, e001770. doi:10.1161/CIRCGENETICS.117.001770

Van Rooij, E., Sutherland, L. B., Liu, N., Williams, A. H., McAnally, J., Gerard, R. D., Richardson, J. A. and Olson, E. N. (2006). A signature pattern of stress-responsive microRNAs that can evoke cardiac hypertrophy and heart failure. *Proc. Natl. Acad. Sci. USA* **103**, 18255-18260. doi:10.1073/pnas.0608791103

van Rooij, E., Quiat, D., Johnson, B. A., Sutherland, L. B., Qi, X., Richardson, J. A., Kelm, R. J. and Olson, E. N. (2009). A family of microRNAs encoded by myosin genes governs myosin expression and muscle performance. *Dev. Cell* **17**, 662-673. doi:10.1016/j.devcel.2009.10.013

Webster, C., Silberstein, L., Hays, A. P. and Blau, H. M. (1988). Fast muscle fibers are preferentially affected in Duchenne muscular dystrophy. *Cell* **52**, 503-513. doi:10.1016/0092-8674(88)90463-1

Westendorp, B., Major, J. L., Nader, M., Salih, M., Leenen, F. H. H. and Tuana, B. S. (2012). The E2F6 repressor activates gene expression in myocardium resulting in dilated cardiomyopathy. *FASEB J.* **26**, 2569-2579. doi:10.1096/fj.11-203174

Williams, A. H., Valdez, G., Moresi, V., Qi, X., McAnally, J., Elliott, J. L., Bassel-Duby, R., Sanes, J. R. and Olson, E. N. (2009). MicroRNA-206 delays ALS progression and promotes regeneration of neuromuscular synapses in mice. *Science* **326**, 1549-1554. doi:10.1126/science.1181046

Winbanks, C. E., Wang, B., Beyer, C., Koh, P., White, L., Kantharidis, P. and Gregorevic, P. (2011). TGF-β regulates miR-206 and miR-29 to control myogenic differentiation through regulation of HDAC4. *J. Biol. Chem.* **286**, 13805-13814. doi:10.1074/jbc.M110.192625

Yang, Y., Del Re, D. P., Nakano, N., Sciarretta, S., Zhai, P., Park, J., Sayed, D., Shirakabe, A., Matsushima, S., Park, Y. et al. (2015). MIR-206 mediates YAP-induced cardiac hypertrophy and survival. *Circ. Res.* **117**, 891-904. doi:10.1161/CIRCRESAHA.115.306624

Yuasa, K., Ando, M., Nakamura, A., Takeda, S., Hagiwara, Y. and Hijikata, T. (2008). MicroRNA-206 is highly expressed in newly formed muscle fibers: implications regarding potential for muscle regeneration and maturation in muscular dystrophy. *Cell Struct. Funct.* **33**, 163-169. doi:10.1247/csf.08022

Yutzey, K. E. and Konieczny, S. F. (1992). Different E-box regulatory sequences are functionally distinct when placed within the context of the troponin I enhancer. *Nucleic Acids Res.* **20**, 5105-5113. doi:10.1093/nar/20.19.5105

Zhai, C., Qian, Q., Tang, G., Han, B., Hu, H., Yin, D., Pan, H. and Zhang, S. (2017). MicroRNA-206 protects against myocardial ischaemia-reperfusion injury in rats by targeting Gadd45β. *Mol. Cells* **40**, 916-924.

Zhao, Y., Samal, E. and Srivastava, D. (2005). Serum response factor regulates a muscle-specific microRNA that targets Hand2 during cardiogenesis. *Nature* **436**, 214-220. doi:10.1038/nature03817